The effects of Jahn–Teller distortion changes on transport properties in $LaMn_{1-x}Zn_xO_3$

2003 J. Phys.: Condens. Matter 15 2033

(http://iopscience.iop.org/0953-8984/15/12/320)

INSTITUTE OF PHYSICS PUBLISHING JOURNAL OF PHYSICS: CONDENSED MATTER

J. Phys.: Condens. Matter **15** (2003) 2033–2043 PII: S0953-8984(03)58400-4

The effects of Jahn–Teller distortion changes on transport properties in $LaMn_{1-x}Zn_xO_3$

Liangbing Hu[1,2], **Wei Tong**[1,2], **Hong Zhu**[1,2] **and Yuheng Zhang**[1,2]

[1] Structure Research Laboratory, University of Science and Technology of China, Hefei 230026, People's Republic of China
[2] National High Magnetic Field Laboratory, Hefei 230031, People's Republic of China

Received 16 January 2003
Published 17 March 2003
Online at stacks.iop.org/JPhysCM/15/2033

Abstract

The magnetism and magnetotransport properties of doped perovskite $LaMn_{1-x}Zn_xO_3$ ($x = 0.05, 0.10, 0.15, 0.20, 0.30, 0.40$) have been studied. All samples exhibit insulating behaviour under zero field and a 6 T field (except for $x = 0.05$, the weak insulating–metallic transition occurs near T_C under zero field), but there is a paramagnetic–ferromagnetic (PM–FM) transition and a large MR effect near T_C. The ρ–T curves are fitted well by a semiconductor-like model. We suggest that the MnO_6 octahedron is contorted by zinc doping and that this contortion will influence the Jahn–Teller (JT) distortion of Mn^{3+}. The e_g carrier has to overcome the energy gap caused by the difference between the JT distortions induced by Mn^{3+} in the non-contorted MnO_6 octahedrons and the contorted ones. Infrared spectra and Raman spectra confirmed our ideas. In addition, the magnetism was investigated by ESR and M–T measurements. The Zn doping suppresses the PM–FM transition and T_C decreases with the increase of dopant. For $x = 0.30$ and 0.40, there exists cluster–glass behaviour in the low-temperature range.

1. Introduction

Due to their significance for both fundamental research and practical application, the magnetoresistance materials of mixed-valence manganites with perovskite structure have been studied for a long time. As we know, $LaMnO_3$ is an antiferromagnetic (AFM) insulator with ABO_3 structure. In this system the manganese ions are all trivalent and Mn^{3+}–O–Mn^{3+} is dominated by the superexchange (SE) interaction. When doped with a certain number of divalent ions in the A sites, $R_{1-x}A_xMnO_3$ (R = rare earth, A = Ca, Sr, Ba [1, 2]), a proportional number of Mn^{3+} ions are converted into Mn^{4+} to balance the valence of the system. For the broad doping range $0.2 \leqslant x \leqslant 0.5$, there is an insulating–metallic (IM) transition associated with the paramagnetic–ferromagnetic (PM–FM) transition. The double exchange (DE) interaction between Mn^{3+} and Mn^{4+} introduced by Zener [3] can explain the

above. Recent studies suggest that the local Jahn–Teller (JT) distortion plays a key role in these manganites [4, 5]. The DE interaction and JT distortion have been generally accepted to explain the mechanism of conduction in mixed-valence manganites.

Doping on Mn sites will destroy the Mn^{3+}–O–Mn^{4+} DE interaction and bring about different results from doping on A sites. Therefore, Mn-site doping has been a focus of study recently and can usually be divided into three categories:

(1) $La_{1-x}A_xMn_{1-y}B_yO_3$ (A = Ca, Sr, Ba and B = Fe [6], Cr [7], Ga [8], Co [9], Al [10]), with x fixed at $1/3$ corresponding to optimal doping (maximal colossal magnetoresistance (CMR) effect) on the A site;
(2) $La_{1-x}A_xMn_{1-y}B_yO_3$ (A = Ca, Sr, Ba and and B = Cr, Co [11], Cu [12], Fe [13]), with x fixed at $1/8$ or $1/2$ corresponding to the charge ordered state;
(3) $LaMn_{1-y}B_yO_3$ (B = Ti [14], Cu [15], Cr [16, 17], Fe [18], Co [19, 20], Ga [21], Zn, Li, Mg, Rh, Ni [22]).

The doped ions on Mn sites not only adjust the Mn^{3+}/Mn^{4+} ratio but also, due to the fact that they may not participate in the DE interaction with Mn^{3+}/Mn^{4+}, destroy the DE interaction between Mn^{3+} and Mn^{4+}. The B ions occupying the Mn site directly block the movement of charge carriers. This is more obvious in heavily doped samples. Upon doping magnetic ions with $t_{2g}^3e_g^1/t_{2g}^3e_g^0$ configuration in the Mn sites, there may exist DE interaction between Mn^{3+}/Mn^{4+} and the magnetic ions. For Cr, Sun *et al* [16] suggested possible DE interaction between Cr^{3+} and Mn^{3+}, while Gundakaram *et al* [17] pointed out that the interaction is of the SE not DE type. For heavy doping on Mn sites with Cu [12, 15], Cu^{2+}–O–Cu^{2+} is formed in the Mn–O plane and is antiferromagnetically ordered in the FM region. The Cu^{2+} ions do not participate in the DE interaction with Mn^{3+}/Mn^{4+}.

Doping on Mn sites is often with magnetic ions and the main goal is to investigate the possible DE and magnetic coupling between the doping ions and the Mn ions. In this paper we choose non-magnetic Zn^{2+} ions, which will not introduce a complicated magnetic background. Due to the small difference in radius between Zn^{2+} (74 pm) and Mn^{3+}(72 pm)/Mn^{4+} (67 pm), some heavily doped samples would be expected and no structural change would be observed. The effects of Zn doping on the magnetotransport behaviour would result from other internal factors rather than structural change. We suggest that the substitution of Zn for Mn will change the JT distortion, which is induced by the Mn^{3+} ions neighbouring Zn, and then result in the PM–FM transition without an IM transition.

2. Experimental details

The samples were prepared by the conventional solid state reaction method with appropriate amounts of La_2O_3, MnO_2 and ZnO as the starting materials. The mixture of these starting materials was heated in air at 900 °C for 12 h, 1000 °C for 12 h and 1180 °C for 24 h with intermediate grinding. After the final grinding they were pressed into pellets and sintered at 1200 °C for 24 h.

X-ray diffraction (XRD) was performed with a Japan Rigaku $D/\max\text{-}\gamma A$ rotating powder diffractometer using Cu Kα radiation. Figure 1 shows that all the samples are of single phase. A structural transition from rhombohedral to orthorhombic is observed when the Zn content exceeds 0.10. The resistivity ρ under zero and 6 T magnetic field was measured by the standard four-probe method with an Oxford 15 T system. A superconducting coil was used to produce a steady magnetic field. Magnetization measurements were performed using a LakeShore vibrating sample magnetometer (VSM). After zero-field cooling (ZFC) and 0.01 T field cooling (FC) down to 5 K, the magnetization data with increase of temperature were

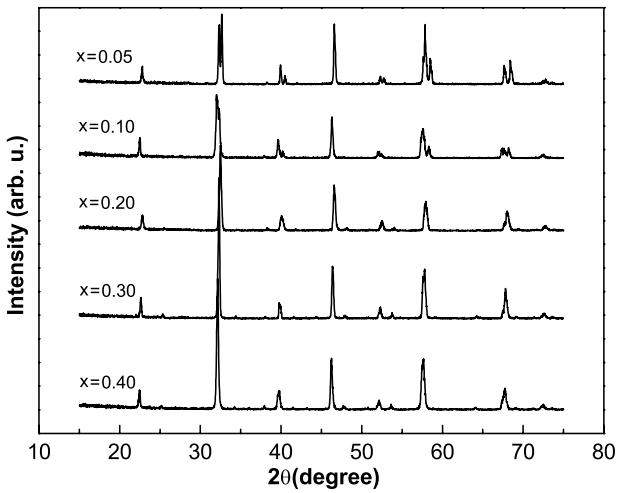

Figure 1. XRD patterns of $LaMn_{1-x}Zn_xO_3$ ($0.05 \leqslant x \leqslant 0.40$).

collected in a 0.01 T field. The micromagnetic properties of the samples were investigated by measurements of electronic spin resonance (ESR) spectra on a Bruker ER200D spectrometer. The limit of the lowest temperature in the ESR system was 100 K and the frequency of the microwave used in the measurements was 9.6 GHz. The measurements of infrared (IR) transmission spectra (Nicolet 700) were carried out at room temperature with powder samples in which KBr was used as a carrier. Raman scattering spectra were obtained on a Spex Ramalog 6 Raman spectrophotometer using a back-scattering technique.

3. Results and discussions

3.1. Magnetism

The magnetization of $LaMn_{1-x}Zn_xO_3$ ($0.05 \leqslant x \leqslant 0.40$) under both ZFC and FC was measured in a 0.01 T magnetic field. Figure 2 shows the dependence of M on temperature (T). The Curie temperature T_C, defined as the temperature corresponding to the peak of dM/dT in the M versus T curve, is 210, 150, 110, 60 and 40 K for $x = 0.05$, 0.10, 0.20, 0.30 and 0.40 respectively. Obviously, T_C decreases with increasing x. A decrease of T_C was also observed in previous studies of Mn-site substitution by Cr [16], Cu [15] and Fe [18], but it is more sensitive to Zn doping. The magnetic ions Cr^{3+}, Cu^{2+} and Fe^{3+}/Fe^{4+}, on the one hand, destroy the DE interaction between Mn^{3+} and Mn^{4+}, and, on the other hand, introduce possible DE interaction between Cr^{3+} and Mn^{3+} or SE interaction between Cu^{2+} ions or SE interaction between Fe^{3+}/Fe^{4+} ions. But non-magnetic Zn^{2+} ions only destroy DE interaction between Mn^{3+} and Mn^{4+}. Therefore, T_C decreases more rapidly for Zn doping. Figure 2 also shows that the PM–FM transition is gradually broadened as x increases. This is the same as for Cr [16], Cu [15] and Fe [18] doping. As mentioned above, the previous papers suggested that this is due to the coupling between the doped ions and the Mn ions or the doped ions themselves. The complicated ferromagnetic clusters in the systems are formed by a combination of the ferromagnetic DE interaction and the AFM SE interaction. $Zn^{2+}(d^{10})$ is not magnetic and is not able to participate in the DE interaction with Mn ions. Zn^{2+} doping on Mn sites creates an equal number of Mn^{4+} and causes the inhomogeneous distribution of Mn^{3+}–O–Mn^{4+}, which results

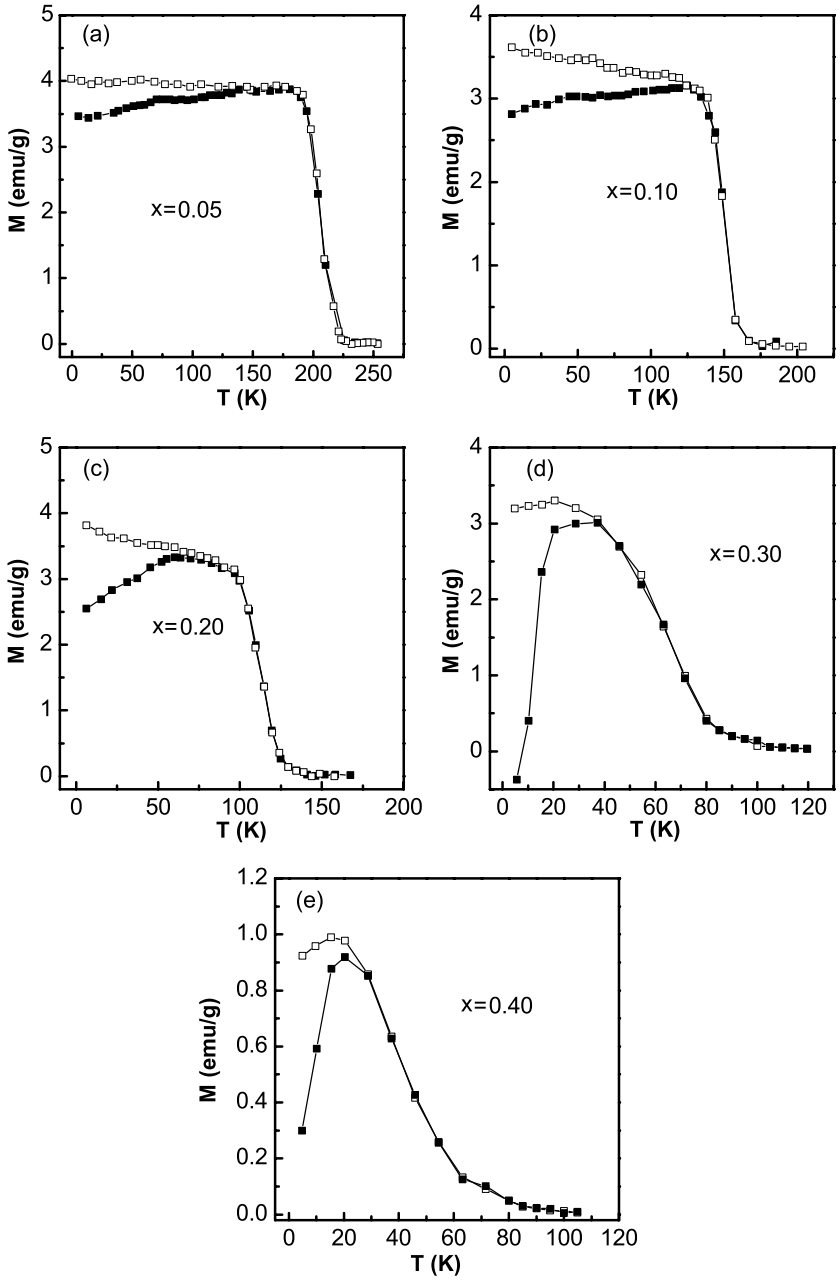

Figure 2. Temperature dependence of M for $LaMn_{1-x}Zn_xO_3$ in a 100 Oe magnetic field.

in short-range ferromagnetic Mn^{3+}–O–Mn^{4+} clusters. The PM–FM transition temperatures for clusters of different sizes are different. In figure 2 the broadening of the PM–FM transition with increasing x represents the collective contribution of all clusters.

For $x \leqslant 0.20$, when $T < T_C$, the M under ZFC decreases slowly and the M under FC increases slowly with decreasing temperature. No clusters form in our samples when

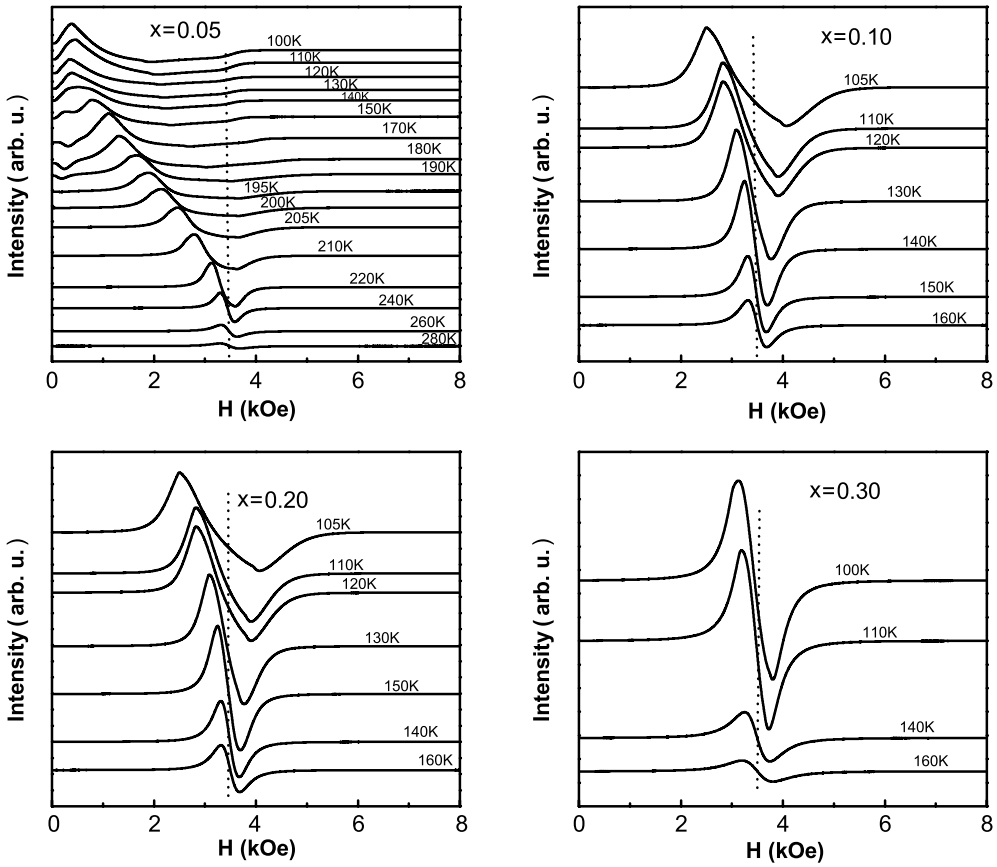

Figure 3. Temperature dependence of the ESR signal for $LaMn_{1-x}Zn_xO_3$ ($x = 0.05$, 0.10, 0.20 and 0.30).

$x \leqslant 0.2$, which can be seen from two aspects. Firstly the M–T curves under ZFC and under FC are not very different, and the M under ZFC changes little with decreasing temperature at $T < T_C$. Secondly the PM–FM transitions in the M–T curves are very sharp. The results of micromagnetic characterization obtained by ESR measurement are shown in figure 3. The typical paramagnetic resonance lines (PL) with a g-factor of approximately 2 were observed in the temperature range $T \geqslant 220$, 160, 130 K, for $x = 0.05$, 0.10, 0.20 respectively, which corresponds to the onset temperature of the PM–FM transition in M–T (figures 2(a)–(c)). Below these temperatures, PL in the three samples disappear quickly and ferromagnetic resonance lines (FL) with $g > 2$ appear. These FL shift to lower field with decreasing temperature. The results of M–T and ESR show the normal PM–FM transition for $x \leqslant 0.20$. While for $x \geqslant 0.30$, the M–T curves under FC are quite different from the ZFC ones and the 'λ' transition was observed, which is characteristic of cluster glass. The ESR spectra of $x = 0.30$ have good PL within the measured temperature range. The reason for this is that the lowest temperature (100 K) of our ESR system is higher than T_C^{onset} (84 K) in the M–T curves of figure 2(e).

In summary, microscopic and macroscopic measurements agree well with each other. For $x \leqslant 0.20$ the PM–FM transition is sharp, and for $x \geqslant 0.30$ the Zn^{2+} doping divides the systems into ferromagnetic clusters.

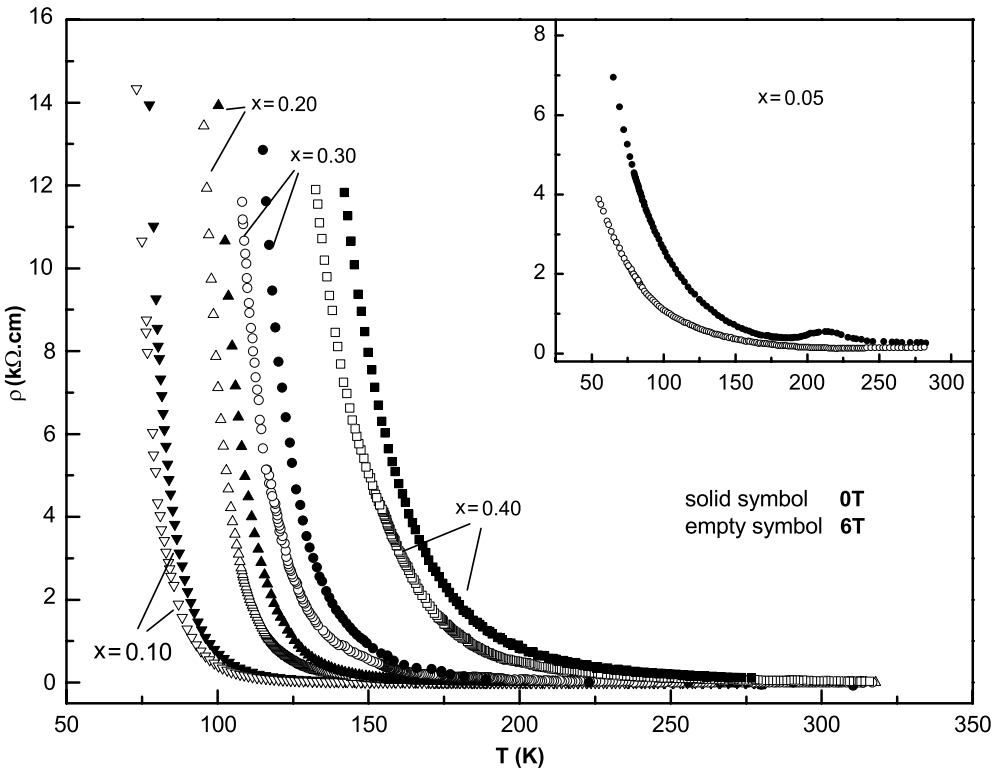

Figure 4. Temperature dependence of resistivity in zero magnetic field and 6 T magnetic field for $LaMn_{1-x}Zn_xO_3$. The inset shows temperature dependence of resistivity for $x = 0.05$ in zero magnetic field and 6 T magnetic field.

3.2. Transport properties

Figure 4 shows the resistivity ρ versus temperature under zero field and 6 T field for the samples $LaMn_{1-x}Zn_xO_3$ ($0.05 \leqslant x \leqslant 0.40$). For $x = 0.05$, there is an IM transition bump near T_C in the ρ–T curve under zero field and the resistivity increases rapidly with cooling after the IM transition. This is also observed in $La_{2/3}Ca_{1/3}Mn_{0.9}Fe_{0.1}O_3$ [23]. The IM transition bump disappears and the ρ–T curve exhibits an insulating behaviour under a 6 T field. For $x \geqslant 0.10$, both under a zero field and a 6 T field, the samples are of insulating behaviour and no IM transition was observed.

It is very common that there is a PM–FM transition but no IM transition in Mn-site doping samples. Many models [24–27] have been used to explain this kind of resistivity behaviour, such as the adiabatic polaron hopping model $\rho \sim T\exp(T_0/T)$, the semiconducting model $\rho \sim \exp(T_0/T)$, the variable range hopping model (VRH) $\rho \sim \exp(T_0/T)^{1/4}$ and VRH of polaron $\rho \sim T\exp(T_0/T + (T_0/T)^{1/4})$. The insulating conductivity in the PM region has been studied in many papers. It is fitted well by the models mentioned above. In the FM region, it is generally considered that the charge carriers have to hop over the potential barrier caused by the ions substituting for Mn. Therefore, the conductivity is dominated by the VRH model. Alternatively, due to the formation of ferromagnetic clusters, the e_g carrier has to overcome the barrier between clusters. The conductivity is metallic within the cluster and is insulating between the clusters. The conductivity between clusters determines the macroscopic resistivity. Therefore insulating behaviour was observed.

However, as interpreted above by micromagnetism and macromagnetism measurements, no clusters form in our samples when $x \leqslant 0.20$. But the ρ–T curve still shows semiconductor-like characteristics in the FM region. Obviously this is not due to the e_g hopping between clusters. We hope to explain the insulating conductivity in the entire temperature range including the FM region. Because polarons are hard to form in an FM background, we choose the semiconducting model and the VRH model rather than the small polaron model to fit the ρ–T curve.

The ρ–T curves are fitted by the semiconducting model and the VRH model in figures 5(a) and (b), respectively. Surprisingly, they are fitted better by the semiconducting model than by the VRH model. In previous studies of Mn-site doping, the VRH model has described the resistivity well. For example, the resistivity is fitted and explained well by VRH at high temperature for $La_{2/3}Ca_{1/3}Mn_{0.9}Fe_{0.1}O_3$ [23]. In figure 5(a) it is interesting that the relations $\ln \rho$–$1/T$ are linear not only for all the samples when $T > T_C$ but also for $x \leqslant 0.2$ when $T < T_C$. But the slopes of the two sets of lines for $T < T_C$ and $T > T_C$ are different and the temperature connecting the two lines agrees well with T_C for $x = 0.10$ and 0.20. The temperature range (0.048–0.01 of $1/T$) corresponds to the IM transition range for $x = 0.05$.

As discussed above, the transport properties in $LaMn_{1-x}Zn_xO_3$ are described well by a thermal activation model, which implies that an energy gap is introduced for the e_g carrier. As we know, the hopping of the e_g carrier between Mn^{3+} and Mn^{4+} in CMR materials has an equal energy state in the framework of the DE interaction with JT distortion. In our samples the e_g electron has to overcome an energy gap. In figure 5(a) we can see that the $\ln \rho$–$1/T$ curves are approximately parallel when $T > T_C$, which indicates that the energy gaps for e_g carrier hopping are the same. We suggest that the MnO_6 octahedron is contorted by zinc doping and this contortion will influence the JT distortion induced by the Mn^{3+} neighbouring the Zn. The e_g carrier has to overcome the energy gap caused by the difference between the JT distortions induced by the Mn^{3+} in the non-contorted MnO_6 octahedron and the contorted one. This can explain why the resistivity of $LaMn_{1-x}Zn_xO_3$ ($x = 0.05$, 0.10, 0.20, 0.30, 0.40) obeys the semiconducting model in the PM region. When $T < T_C$, the JT distortion disappears. However, the energy level of the e_g orbital in a contorted MnO_6 octahedron still differs from that in a non-contorted MnO_6 octahedron, and so the ρ–T relation still obeys the semiconducting model, not the metallic model. To confirm our ideas, we studied the IR spectra and the Raman spectra.

For the ABO_3 structure, IR and Raman absorption comes from the collective vibration mode of MnO_6. The six typical vibration modes can be obtained from the equation $H\Psi = E\Psi$ [28]. Among the six modes, ν_3 and ν_4 are IR activated. These two vibration modes appear in the IR spectra of figure 6(a). With increasing x, ν_3, which corresponds to the stretching vibration mode in the vertical plane, does not change, while ν_4, which corresponds to the bending vibration mode in the horizontal plane, is strengthened and shifts to slightly higher wavenumbers. The result implies that the MnO_6 octahedrons neighbouring the Zn are contorted in the horizontal plane. At the same time the Raman spectra were measured and are shown in figure 6(b). The absorption peaks appear not only around 500 cm^{-1} but also around 615 cm^{-1}, which correspond to the A_g (JT mode) and B_g (breathing mode) respectively [29, 30]. They correspond to vibration in the horizontal plane. With increasing x, the wavenumbers of the two peaks do not change but the strength increases. The occurrence and the strengthening of the two peaks with increasing x also indicate that the MnO_6 octahedrons are contorted in the horizontal plane. The Raman spectra results agree with those of the IR spectra. The contortion will influence the JT distortion induced by Mn^{3+}. The JT distortion in the contorted MnO_6 octahedron is different from that in the non-contorted one. Due to the difference in

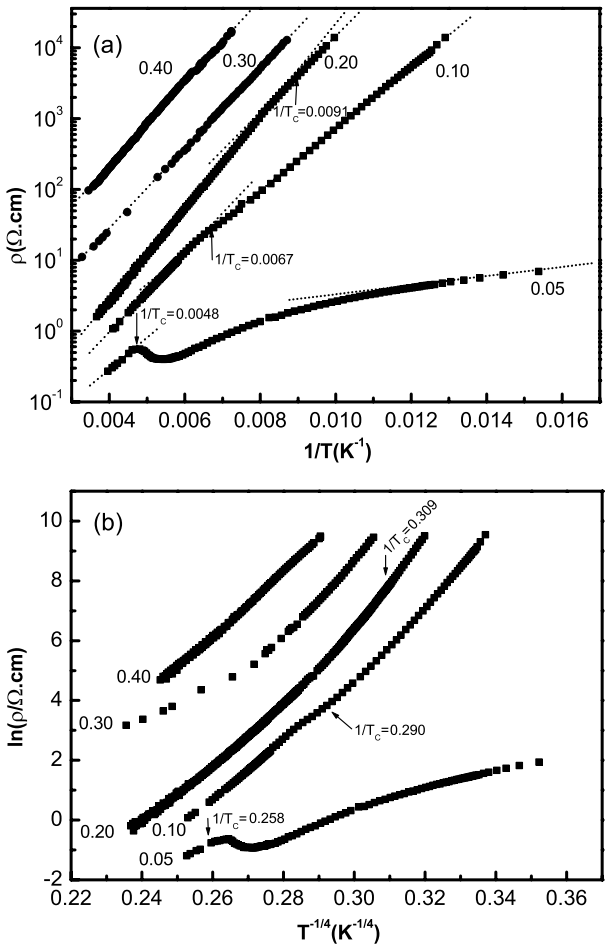

Figure 5. (a) $\ln(\rho)$ is plotted against inverse temperature for $LaMn_{1-x}Zn_xO_3$. (b) $\ln(\rho)$ is plotted against $T^{(-1/4)}$ for $LaMn_{1-x}Zn_xO_3$.

JT distortions of Mn^{3+}, the energy gap for the e_g carrier is introduced and semiconductor-like behaviour occurs.

Now we return to discuss the fitting curves in figure 5(a). With increasing x, the number of contorted MnO_6 octahedrons increases. However, the likelihood that any contorted MnO_6 octahedron leads to JT distortion is the same. The energy gap keeps constant as x increases. So the slope coefficients of ρ–T above T_C are approximately the same. Also, as mentioned in [31, 32], the ordered arrangement of the magnetic moments of Mn ions in the FM region releases the internal pressure. Therefore the contortion of the MnO_6 octahedral structure disappears. As the content of doped Zn increases, the degree of the ordered arrangement of the magnetic moments of Mn ions is weakened and the contortion of the MnO_6 octahedron is strengthened. So the e_g levels for different samples are different and the slope coefficients at $T < T_C$ are different.

In figure 7 we depict the dependence of MR on temperature for $x = 0.05$, 0.10 and 0.20, where MR is defined as $\mathrm{MR} = [\rho(0) - \rho(H)]/\rho(H)$. The MR peak around T_C is broadened. This may be due to ferromagnetic clusters in the samples. The MR effect is greater than that

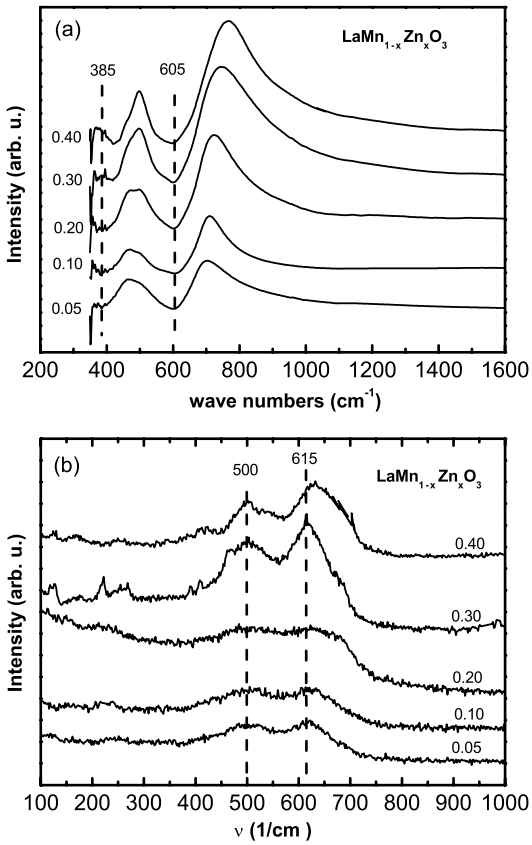

Figure 6. (a) IR phonon spectra of $LaMn_{1-x}Zn_xO_3$ compounds at room temperature. (b) Raman spectra of $LaMn_{1-x}Zn_xO_3$ compounds at room temperature.

of the other Mn-site doped manganites, such as Cu [15], Fe [18] and Cr [16] systems. For $x = 0.05$, the MR is up to 270% around T_C.

4. Conclusion

The magnetism and magnetotransport properties of doped $LaMn_{1-x}Zn_xO_3$ ($0 \leqslant x \leqslant 0.40$) perovskite were studied. All samples exhibit insulating behaviour under zero field and 6 T field (except for $x = 0.05$, the IM transition trend occurs near T_C under zero field), but there is a PM–FM transition and MR effect near T_C. Strangely, we found that the ρ–T relation is fitted better by the semiconducting model than by the VRH model. It is more interesting that the relation $\ln \rho$–$1/T$ is linear not only for all the samples when $T > T_C$ but also for $x \leqslant 0.2$ when $T < T_C$. It is just T_C that separates the $\ln \rho$–$1/T$ curve into two sets of lines. We suggest that the MnO_6 octahedron is contorted by zinc doping and this contortion will influence the JT distortion of Mn^{3+} neighbouring Zn. The e_g carrier has to overcome the energy gap, which is caused by the difference between the JT distortions induced by the Mn^{3+} in the non-contorted MnO_6 octahedron and the contorted one. When $T < T_C$, the JT distortion disappears. However, the e_g level in contorted MnO_6 octahedron still differs from that in non-contorted MnO_6 octahedrons and the ρ–T relation still obeys the semiconducting

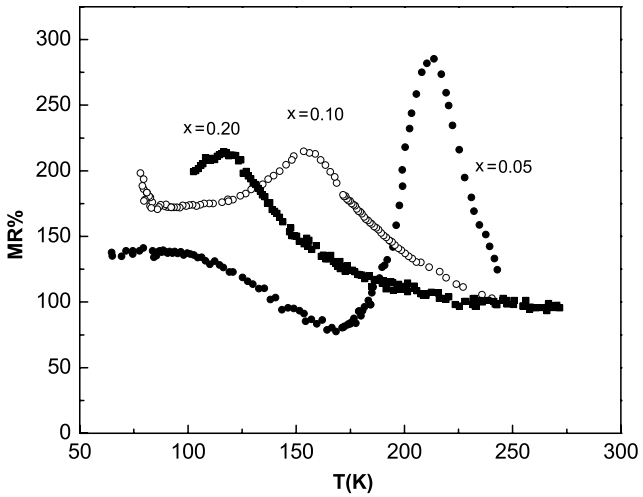

Figure 7. Temperature dependence of magnetoresistance for $LaMn_{1-x}Zn_xO_3$ samples ($x = 0.05$, 0.10 and 0.20) in a 6 T magnetic field.

model and not the metallic one in the FM region. The IR and Raman spectra confirmed out ideas.

Acknowledgment

The authors would like to thank Dr Deliang Zhu, Shiyan Li and Changjin Zhang, for their help in experiments. The authors also thank Miss Gong Fei for typesetting this manuscript. This work was supported by the National Nature Science Foundation of China (no 19934003) and the State Key Project of Fundamental Research, China (001CB610604).

References

[1] Von Helmolt R, Wecker J, Holzapfel B, Schultz M and Samwer K 1993 *Phys. Rev. Lett.* **71** 2331
[2] Jin S, Tiefel T H, McCormack M, Fastnacht R A, Ramesh R and Chen L H 1994 *Science* **264** 413
[3] Zener C 1951 *Phys. Rev.* **82** 403
[4] Millis A J, Littlewood P B and Shramiman B I 1995 *Phys. Rev. Lett.* **74** 3407
[5] Jahn H A and Teller E 1937 *Proc. R. Soc.* A **161** 220
[6] Ahn K H, Wu X W, Liu K and Chien C L 1996 *Phys. Rev.* B **54** 15299
[7] Sun Y, Xu X J and Zhang Y H 2000 *Phys. Rev.* B **63** 54404
[8] Sun Y, Xu X J, Zheng L and Zhang Y H 1999 *Phys. Rev.* B **60** 12317
[9] Gayathri N, Raychaudhuri A K and Tiwary S K 1997 *Phys. Rev.* B **56** 1345
[10] Blasco J, García J, de Teresa J M, Ibarra M R, Perez J, Algarabel P A and Marquina C 1997 *Phys. Rev.* B **55** 8905
[11] Raveau B, Maigan A and Martin C 1997 *J. Solid State Chem.* **130** 162
[12] Pi L, Xu X J and Zhang Y H 2000 *Phys. Rev.* B **62** 5667
[13] Ogale S B, Shreekala R, Bathe R, Date S K, Patil S I, Hannoyer B, Petit F and Marest G 1998 *Phys. Rev.* B **57** 7841
[14] Kutty T R N and Philip J 2000 *J. Phys.: Condens. Matter* **12** 7747
[15] Sun Y, Xu X J, Tong W and Zhang Y H 2000 *Appl. Phys. Lett.* **77** 2734
[16] Sun Y, Tong W, Xu X J and Zhang Y H 2001 *Phys. Rev.* B **63** 174438
[17] Gundakaram R, Arulraj A, Vanitha P V, Rao C N R, Gayathri N, Raychaudhuri A K and Cheetham A K 1996 *J. Solid State Chem.* **127** 354

[18] Tong W *et al* 2003 *Phys. Rev.* B submitted
[19] Park J-H, Cheong S-W and Chen C T 1997 *Phys. Rev.* B **55** 11072
[20] Yang Z Q, Ye L and Xie X D 1999 *Phys. Rev.* B **59** 7051
[21] Goodenough J B, Wold A, Arnott R J and Menyuk N 1961 *Phys. Rev.* **124** 373
[22] Hébert S, Martin C, Maignan A, Retoux R, Hervieu M, Nguyen N and Raveau B 2002 *Phys. Rev.* B **65** 104420
[23] Cai J-W, Wang C, Shen B-G, Zhao J-G and Zhan W-S 1997 *Appl. Phys. Lett.* **71** 1727
[24] Snyder G J, Hiskes R, DiCarolis S, Beasley M R and Geballe T H 1996 *Phys. Rev.* B **53** 14434
[25] Worledge D C, Synder G J, Beasley M R, Geballe T H, Hiskes R and DiCarolis 1996 *J. Appl. Phys.* **80** 5158
[26] Helmolt R, Von Wecker J, Samwer K, Haupt L and Bärner K 1994 *J. Appl. Phys.* **76** 6925
Fontcuberta J, Martínez B, Seffar A, Piñol S, García-Muñoz J L and Obradors X 1996 *Phys. Rev. Lett.* **76** 1122
[27] Sun Y, Xu X J and Zhang Y H 2000 *J. Phys.: Condens. Matter* **12** 10475
[28] Nakamoto K (ed) 1986 *Infrared and Raman Spectra of Inorganic and Coordination Compounds* 4th edn (New York: Wiley–Interscience)
[29] Iliev M N, Abrashev M V, Lee H-G, Popov V N, Sun Y Y, Thomsen C, Meng R L and Chu C W 1998 *Phys. Rev.* B **57** 2872
[30] Martín-Carrón L and de Andrés A 2001 *J. Alloys Compounds* **323/324** 417
[31] Kim K H, Gu J Y, Choi H S, Park G W and Noh T W 1996 *Phys. Rev. Lett.* **77** 1877
[32] Lanzara A, Saini N L, Brunelli M, Natali F and Cheong S-W 1998 *Phys. Rev. Lett.* **81** 878